Investigation of Hot Corrosion Resistance in CNT-Reinforced ZrO_2-Y_2O_3 Composite Coatings on Boiler Tube Steel

Neeluri Suresh[a], Suraj Bhan[b]
[a] Research Scholar, Department of Mechanical Engineering, Noida International University (NIU), Greater Noida
[b]Assistant Professor, Department of Mechanical Engineering, Noida International University (NIU), Greater Noida,

Abstract

Boiler tube failures in Indian thermal power plants are primarily caused by molten sulfates and vanadates, which lead to material degradation at elevated temperatures. Thermal spray coatings are employed as a preventive measure to mitigate such high-temperature corrosion. This study focuses on evaluating the hot corrosion performance of carbon nanotube (CNT)-reinforced ZrO_2-Y_2O_3 composite coatings on T-91 boiler tube steel in a molten salt environment at 900 °C over 50 cycles.The coatings were applied using a plasma spray technique. Test samples underwent hot corrosion testing in a silicon tube furnace at 900 °C for 50 cycles. Post-experiment analysis of the samples was performed using X-ray diffraction, scanning electron microscopy coupled with energy-dispersive spectroscopy, and cross-sectional analysis to understand the corrosion mechanism.The CNT-reinforced coatings demonstrated reduced weight gain during testing, indicative of superior corrosion resistance. The formation of protective oxide scales was observed, and the corrosion resistance improved with higher CNT content in the coating matrix.To the best of the authors' knowledge, the high-temperature behavior of CNT-reinforced ZrO_2-Y_2O_3 coatings on T-91 steel at 900 °C in a molten salt environment has not been previously explored. This research provides valuable insights into the potential use of CNT-reinforced composite coatings for high-temperature applications.

Keywords: High-temperature corrosion, Plasma-sprayed coatings, Carbon nanotubes (CNT), Boiler tube steel, Thermal power plants, ZrO_2-Y_2O_3 composites, Molten salt corrosion.

1. Introduction

At high operating temperatures (around 900°C), as encountered in thermal power plants, traditional alloy steels are unable to perform reliably due to contamination from low-grade fuels (Goyal et al., 2018b; Rani et al., 2017). This issue is often exacerbated by a phenomenon known as hot corrosion, which is a significant challenge in industrial settings such as power plants, gas turbines, and internal combustion engines (Sidhu et al., 2017; Singh et al., 2021). According to Eliaz et al. (2002), hot corrosion is caused by the interaction of salt deposits with the material, leading to the degradation of protective oxide layers and the formation of cracks at grain boundaries due to molten deposits. For instance, sodium vanadyl vanadates are commonly found on boiler superheater tubes, where they degrade steel alloys when in prolonged contact above their melting point of 550°C (Rani et al., 2017).

This process accelerates material deterioration, leading to failures of critical components in power plants, resulting in extended shutdowns and substantial financial losses (Gond et al., 2010). Sidhu and Prakash (2005) reported that high-temperature corrosion accounts for over 50% of boiler tube failures in Indian thermal power plants. The conventional materials used for these applications lack the necessary resistance to withstand such corrosive environments. Schroeder and Unger (1997) recommended thermal spray coatings as an effective solution for protecting alloy steels against high-temperature corrosion.

Thermal spray techniques allow the deposition of thermally stable composite coatings, which shield the substrate material from corrosive agents (Rezakhani, 2007; Singh et al., 2018). Coatings with significant thickness can be produced using methods such as air plasma spray, high-velocity oxy-fuel (HVOF), or arc and flame spraying. Among these, plasma spraying has been identified as a versatile and effective process for enhancing the high-temperature corrosion resistance of boiler components (Erickson et al., 1998). Plasma-sprayed coatings have been found to exhibit properties such as high hardness, low porosity, good adhesion strength, and excellent thermal stability (Jambagi and Bandyopadhyay, 2017). Carbon nanotubes (CNTs), first discovered by Iijima in 1991, have gained significant attention due to their exceptional thermal, electrical, and mechanical properties. Some studies suggest that CNTs possess tensile strength nearly 100 times greater than high-strength steel, along with five times the Young's modulus. These outstanding properties, combined with advancements in synthesis techniques, have facilitated the use of CNTs as reinforcement materials for ceramics, polymers, and metals. CNT-reinforced coatings, such as those used for thermal-sprayed Al_2O_3 and hydroxyapatite, have demonstrated improved hot corrosion resistance on substrates used in boiler steel applications (Goyal et al., 2019).

Thermal spray coatings, despite their advantages, are inherently porous, which allows corrosive species to penetrate and initiate corrosion at the substrate level (Bengtsson and Johannesson, 1995; Kamal et al., 2009). However, incorporating CNTs into these coatings helps fill voids due to their nanoscale size, thereby reducing porosity. This reinforcement enhances both corrosion resistance and wear strength, even at ambient temperatures (Guo and Tam, 2014; Gutierrez-Gonzalez et al., 2015).

This research aims to investigate the hot corrosion performance of traditional ZrO_2-Y_2O_3 coatings and CNT-reinforced ZrO_2-Y_2O_3 coatings (with varying CNT contents: 0.5, 1, 2, 4, and 6 wt.%) on T-91 boiler tube steel under laboratory-simulated conditions using a SiC tube furnace at 900°C. Limited studies exist on the high-temperature behavior of these coatings, making this work essential for gaining deeper insights into their performance.

2. Experimentation and Methodology

2.1 Development of Coatings

T-91 boiler tube steel was chosen as the substrate material for this study due to its widespread use in manufacturing boiler and superheater tubes for high-temperature applications. Fresh T-91 steel tubes were sourced from the Talwandi Sabo Thermal Power Plant, Bathinda, Punjab, India. The chemical composition of T-91 steel, determined in weight percentages, was as follows: 0.12 C, 0.42 Si, 0.42 Mn, 0.016 P, 0.004 S, 8.354 Cr, 0.93 Mo, 0.22 Ni, 0.05 V, with the remainder being Fe. Test specimens were cut into dimensions of 22 mm × 15 mm × 3 mm, cleaned with acetone to remove surface impurities, and dried using hot air.

Feedstock powders were prepared by blending zirconium yttrium powder with CNTs in proportions of 0.5, 1, 2, 4, and 6 wt.%. These powders were subsequently used to apply coatings to T-91 steel substrates using plasma spray technology at Metallizing Equipment Comp. Pvt. Ltd., Jodhpur, Rajasthan, India. The coatings, with thicknesses ranging between 250–270 µm, were measured using a Minitest-2000 thickness gauge. The porosity levels were assessed using a LEICA image analyzer. The porosity of traditional ZrO_2-Y_2O_3 coatings was determined to be 4.25%, which decreased with increasing CNT content. Porosity values for 0.5, 1, 2, 4, and 6 wt.% CNT coatings were found to be 3.78%, 3.62%, 3.52%, 3.45%, and 2.93%, respectively, as detailed in Table 1.

2.2 Hot Corrosion Studies in a Molten Salt Environment

Uncoated and coated T-91 steel specimens were cleaned with acetone and dried with hot air to eliminate dust and moisture. The specimens were preheated at 250°C for 2 hours in an oven. A multilayer coating of Na_2SO_4 – 60 wt.% V_2O_5 salt, mixed with distilled water, was applied to the surface of each specimen using a camel hairbrush. The salt deposition was maintained at 3–5 mg/cm² to simulate conditions encountered in actual boiler environments.

The coated specimens were dried at 100°C for 3 hours, after which their weights were recorded using a digital balance. The samples were then placed in alumina boats and subjected to cyclic hot corrosion testing in a silicon tube furnace. Each cycle involved heating the specimens at 900°C for 1 hour, followed by cooling to room temperature for 20 minutes.

Weight measurements were taken after each cycle to monitor corrosion progress. After the tests, the corroded specimens were analyzed using X-ray diffraction (XRD), scanning electron microscopy (SEM), and energy-dispersive spectroscopy (EDS) to study the morphology and composition of the corrosion products.

3. Results

3.1 Visual Observations

Macrographs of both uncoated and coated T-91 steel specimens before hot corrosion tests are shown in Figure 1(i)–(vii). Post-exposure images after 50 cycles of hot corrosion at 900°C in a molten salt environment are depicted in Figure 2(a)–2(g).

For the uncoated T-91 steel, scale formation began after the second cycle and progressively thickened over subsequent cycles. By the 25th cycle, cracks appeared, and by the end of the 50 cycles, the scale exhibited a thick, multilayered structure that was lustrous but fragile and porous. The dark grey discoloration of the specimen indicated severe corrosion, as shown in Figure 2(a).

In the case of the conventional ZrO_2-Y_2O_3-coated specimen, cracks started forming around the 17th cycle and worsened, eventually leading to peeling of the coating near the edges by the final cycle (Figure 2(b)).

For the 0.5% CNT-ZrO_2-Y_2O_3-coated specimen, minor coating swelling and small corner cracks were noted (Figure 2(c)). The CNT-reinforced coatings containing 1%, 2%, 4%, and 6% CNTs (Figures 2(d)–2(g)) displayed lustrous surfaces by the 12th cycle, which remained intact and free from spallation through the entire testing period. The oxide scale on these specimens was smooth, dense, and homogeneous, providing robust protection against hot corrosion.

Table 1. Composition of coating and porosity

Coating	Composition (Wt.%)	Porosity (%)
$ZrO_2Y_2O_3$	100%$ZrO_2Y_2O_3$	4.25
$ZrO_2Y_2O_3$–0.5%CNT	99.5%$ZrO_2Y_2O_3$10.5%CNT	3.78
$ZrO_2Y_2O_3$–1%CNT	99%$ZrO_2Y_2O_3$11% CNT	3.62
$ZrO_2Y_2O_3$–2%CNT	98%$ZrO_2Y_2O_3$12%CNT	3.52
$ZrO_2Y_2O_3$–4%CNT	96%$ZrO_2Y_2O_3$14%CNT	3.45
$ZrO_2Y_2O_3$–6%CNT	94%$ZrO_2Y_2O_3$16%CNT	2.93

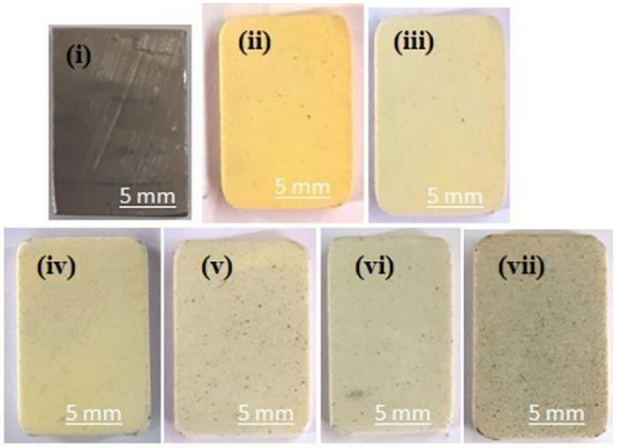

Figure 1. Macrographs of (a) un-coated, (b) $ZrO_2Y_2O_3$, (c) 0.5%CNT-$ZrO_2Y_2O_3$, (d) 1%CNT $ZrO_2Y_2O_3$, (e) 2%CNT-$ZrO_2Y_2O_3$, (f) 4%CNT-$ZrO_2Y_2O_3$ and (g) 6%CNT-$ZrO_2Y_2O_3$- coated T-91 steel specimens before corrosion

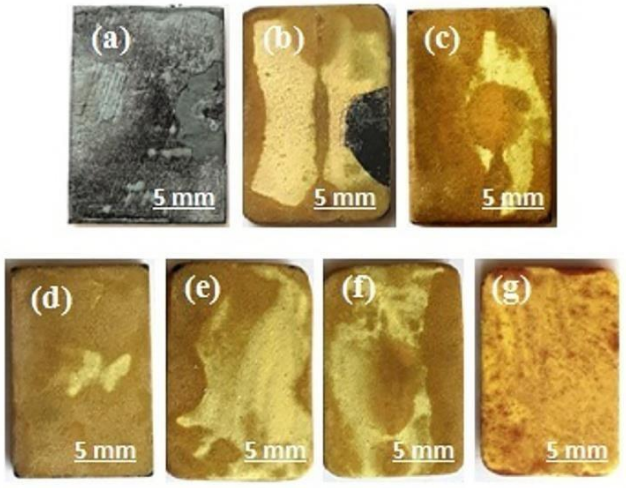

Figure 2. Macrographs of (a) un-coated, (b) $ZrO_2Y_2O_3$, (c) 0.5%CNT-$ZrO_2Y_2O_3$, (d) 1%CNT-$ZrO_2Y_2O_3$, (e) 2%CNT-$ZrO_2Y_2O_3$, (f) 4%CNT-$ZrO_2Y_2O_3$ and (g) 6% CNT-ZrO_2 Y_2O_3-coated T-91 steel specimens after hot corrosion testing at 900°C

3.2 Weight Change Analysis

Weight gain analysis for the uncoated T-91 steel specimen, shown in Figure 3, revealed a consistent increase beginning in the second cycle and continuing linearly through the 50th cycle.

Figure 4 highlights the enhanced corrosion resistance offered by CNT-reinforced ZrO_2-Y_2O_3 coatings. The specimen with the highest CNT content exhibited the lowest weight gain, indicating that increasing CNT percentage improves corrosion resistance.

Figure 5 presents the weight gain per unit area over the 50-cycle exposure period for the uncoated T-91 steel. The uncoated specimen displayed deviations from the parabolic rate law, indicating a rapid degradation. In contrast, the ZrO_2-Y_2O_3-coated and CNT-reinforced coatings followed a parabolic rate trend, as illustrated in Figure 6.

The parabolic rate constant (Kp), calculated from the linear regression slope, is shown in Table 2. The uncoated specimen had significantly higher Kp values compared to all coated specimens. Notably, the cumulative weight gain decreased with an increase in CNT

percentage in the coatings. The ZrO_2-Y_2O_3-6% CNT coating exhibited the lowest parabolic rate constant (Kp = 4.31×10^{-10} g^2 cm^{-4} s^{-1}), indicating superior resistance to hot corrosion.

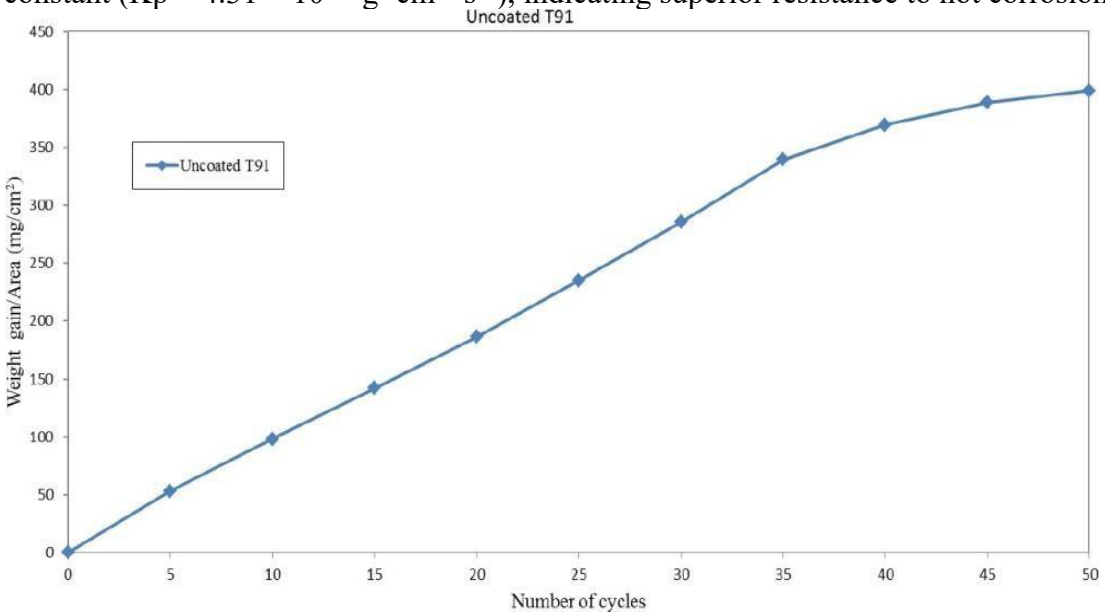

Figure 3.Weight gain / area vs time (number of cycles) forum – coated T-91 specimen after hot corrosion

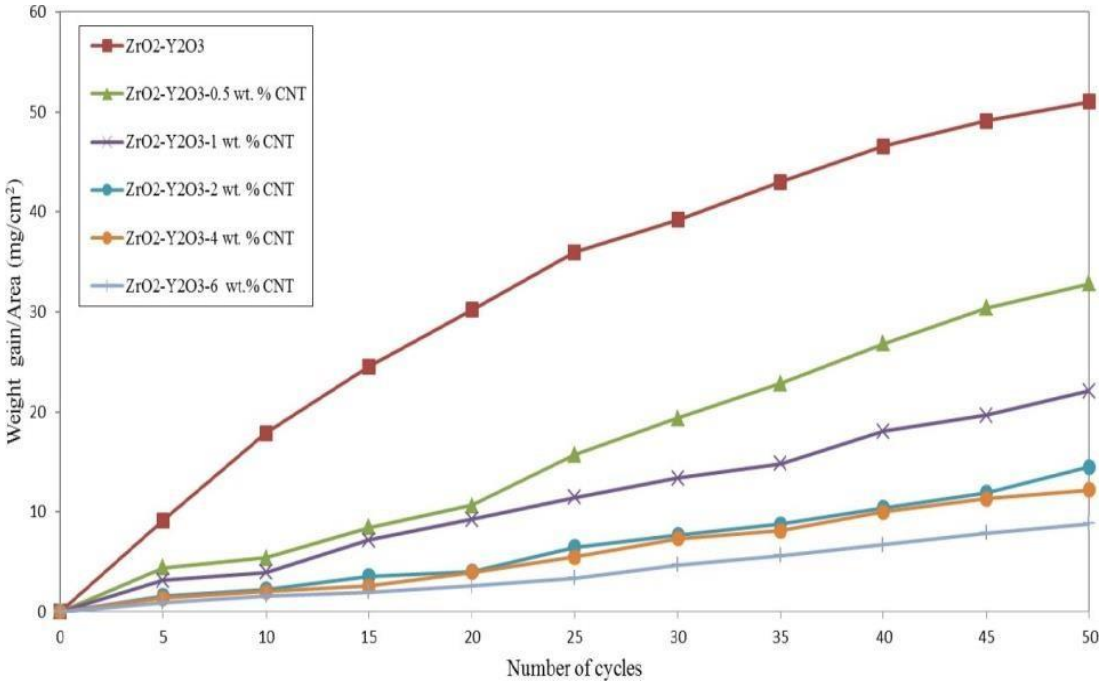

Figure 4. Weight gain / area vs time (number of cycles) for all as-coated samples after hot corrosion

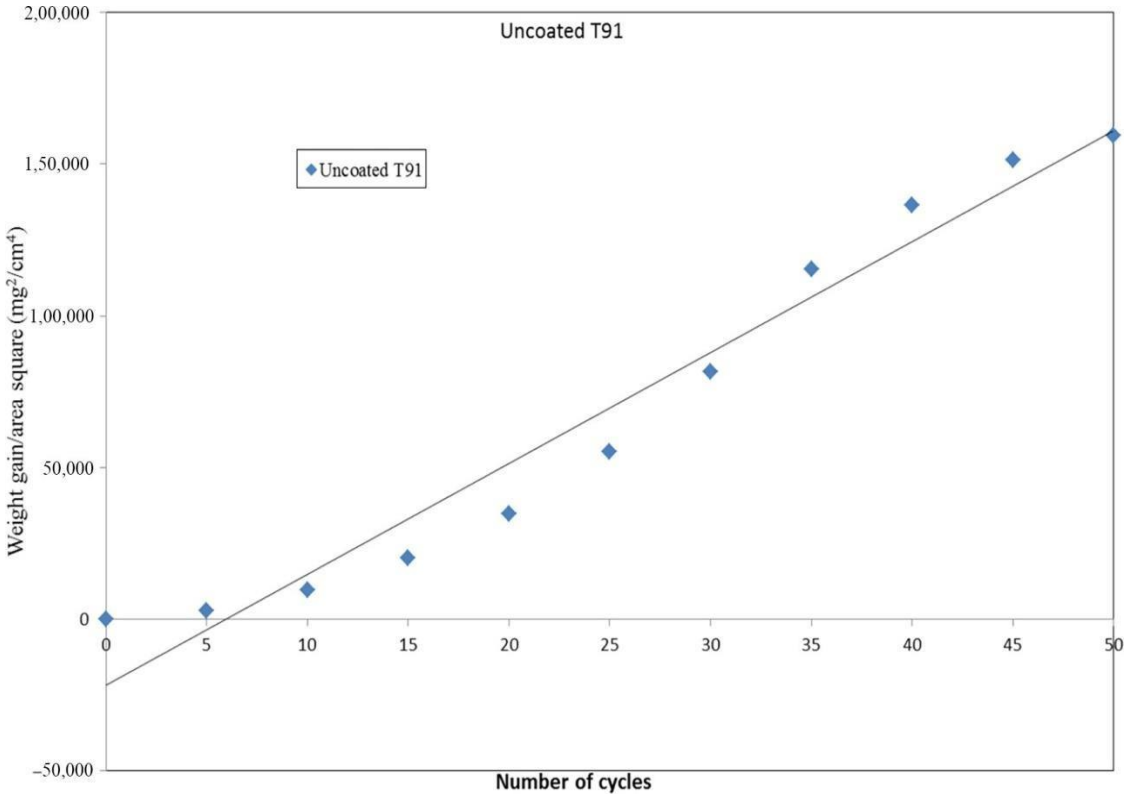

Figure 5. Shows (weight gain / area)^2 versus number of cycles forun-coated T-91 specimen after hot corrosion

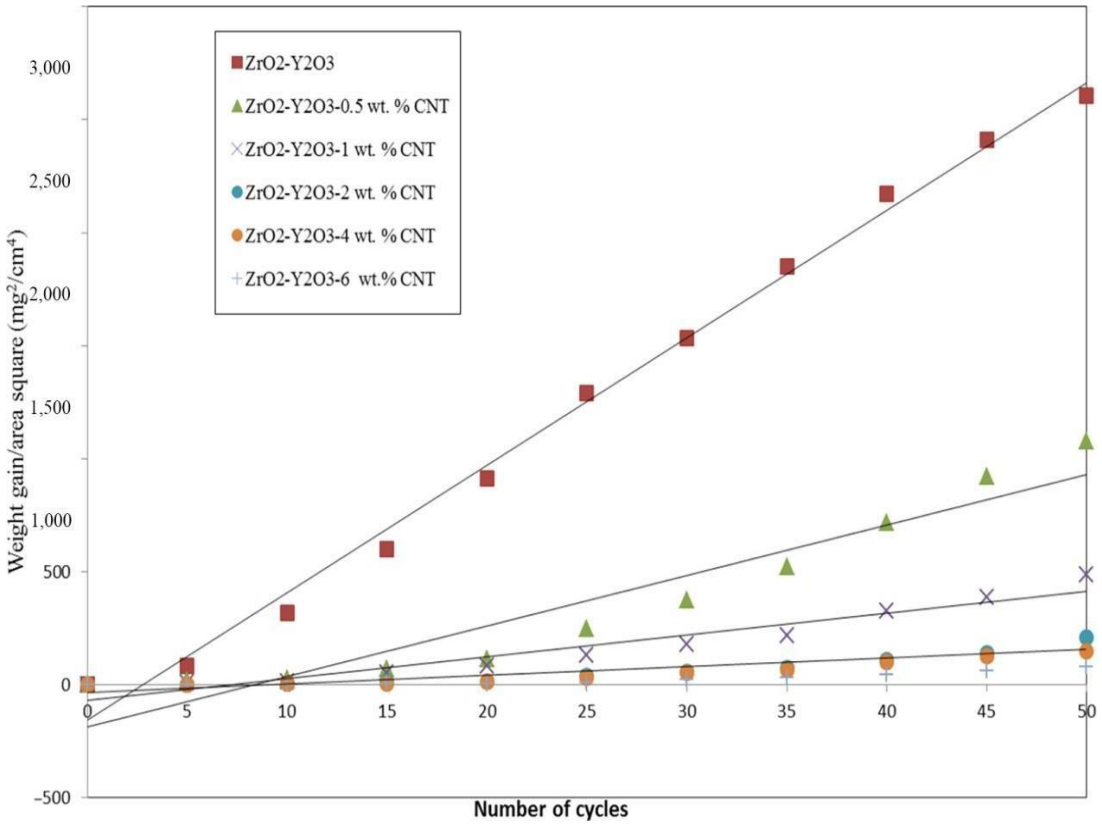

Figure 6. (Weight gain / area)^2 versus number of cycles for all samples after hot corrosion

Table 2. Parabolic rate constant and cumulative weight gain for all samples

Type of coating	K_p values (10^{-10} $g^2cm^{-4}s^{-1}$)	Total weight (cumulative) gain (mg/cm^2)
Uncoated T-91	8,849.82	399.12
ZrO_2-Y_2O_3	144.67	51.03
ZrO_2-Y_2O_3 – 0.5 Wt.% CNT	59.91	32.84
ZrO_2-Y_2O_3 – 1 Wt.% CNT	27.14	22.10
ZrO_2-Y_2O_3 – 2 Wt.% CNT	11.69	14.51
ZrO_2-Y_2O_3 – 4 Wt.% CNT	8.25	12.19

3.3 X-Ray Diffraction (XRD) Analysis

The XRD spectra of uncoated, conventional ZrO_2-Y_2O_3-coated, and CNT-reinforced ZrO_2-Y_2O_3-coated T-91 specimens after high-temperature exposure are shown in Figures 7(a)–7(g). For the uncoated specimen, Fe_2O_3 was identified as the primary phase, with minor amounts of Cr_2O_3 also present, indicating extensive oxidation during exposure (Figure 7(a)). The conventional ZrO_2-Y_2O_3-coated specimen exhibited ZrO_2-Y_2O_3 as the dominant phase, with traces of Cr_2O_3 and Fe_2O_3 detected as secondary phases (Figure 7(b)). XRD analysis confirmed the presence of all elements from the molten salt used in the experiment. The reinforced coatings showed significant improvement in corrosion resistance due to the formation of stable oxide scales, which were dense and adherent, thereby mitigating further degradation.

3.4 Scanning Electron Microscopy (SEM) and Energy Dispersive X-ray Analysis (EDAX)

The SEM micrographs and EDAX analyses of uncoated, conventional ZrO_2-Y_2O_3-coated, and CNT-reinforced ZrO_2-Y_2O_3-coated T-91 steel specimens after hot corrosion at 900°C in a molten salt environment are presented in Figure 8.

Uncoated T-91 Steel

The oxide scale on the uncoated T-91 steel was porous and exhibited a nodular morphology, as shown in Figure 8(a). This scale was identified as non-protective and prone to corrosion. EDAX compositional analysis revealed a significant presence of Fe and O, with notable amounts of Na and V, and minor traces of Cr and Mo. The analysis suggested the formation of oxides, primarily Fe_2O_3, along with oxides of Na, V, Cr, and Mo. The scale's porous and fragile structure indicated poor resistance to high-temperature corrosion.

Conventional ZrO_2-Y_2O_3-Coated T-91 Steel

The SEM image for the conventional ZrO_2-Y_2O_3-coated specimen (Figure 8(b)) revealed the formation of a porous oxide scale with macrovoids. EDAX analysis indicated that Zr and O were the predominant elements, along with Fe and traces of Si. The Si likely diffused through the oxide layer's pores during hot corrosion, potentially forming SiO_2. The presence of Na and V suggested infiltration of molten salt components during the experiment. The scale was less protective compared to CNT-reinforced coatings, as evidenced by its porous morphology.

ZrO_2-Y_2O_3-0.5 wt.% CNT-Coated T-91 Steel

The SEM image of the 0.5 wt.% CNT-reinforced ZrO_2-Y_2O_3-coated specimen (Figure 8(c)) revealed a more compact oxide scale compared to the conventional coating. EDAX

analysis identified Zr and O as major constituents, along with Na, V, and C. The presence of carbon confirmed that CNTs were retained within the oxide layer even after exposure, contributing to the scale's structural integrity.

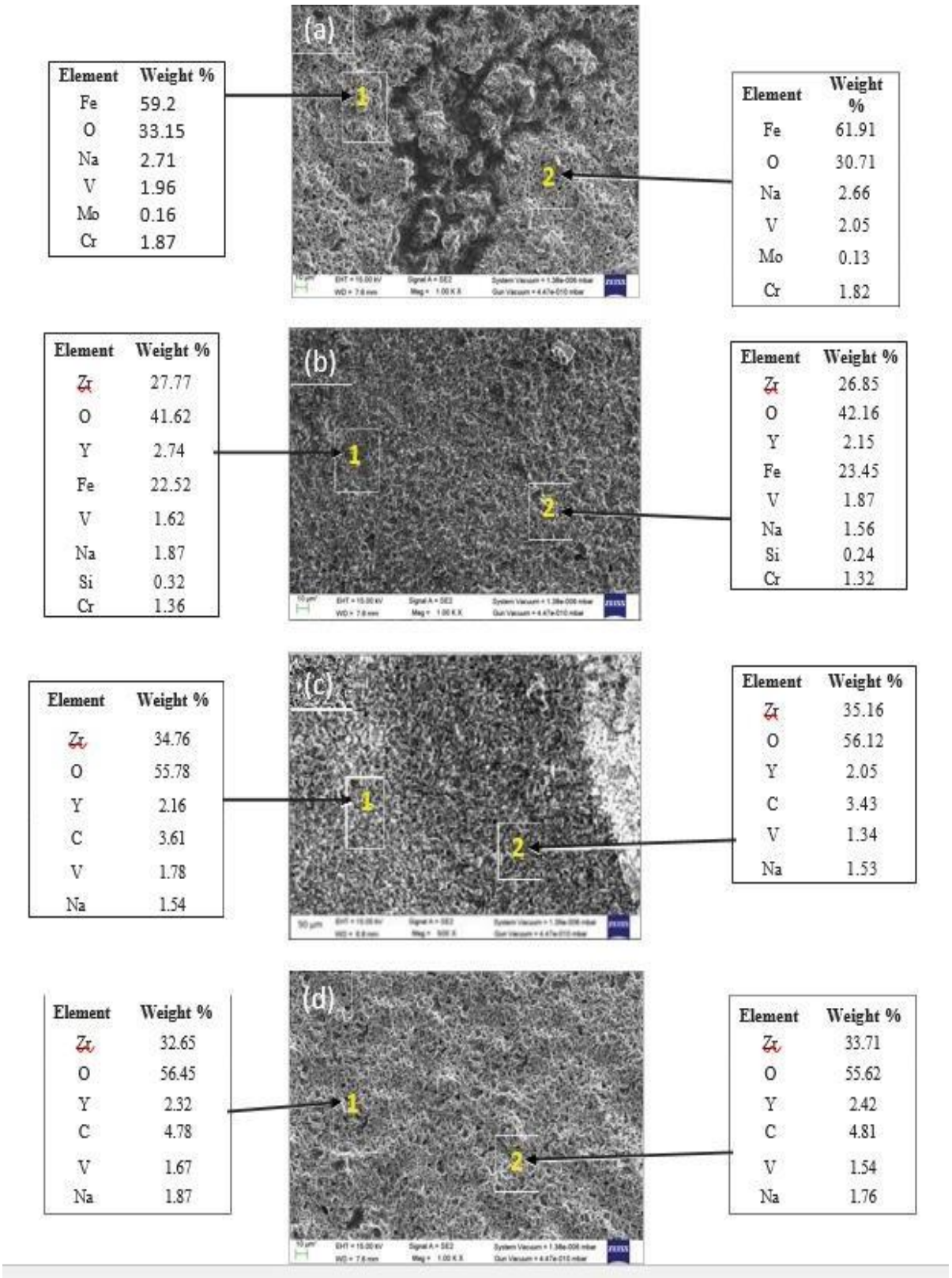

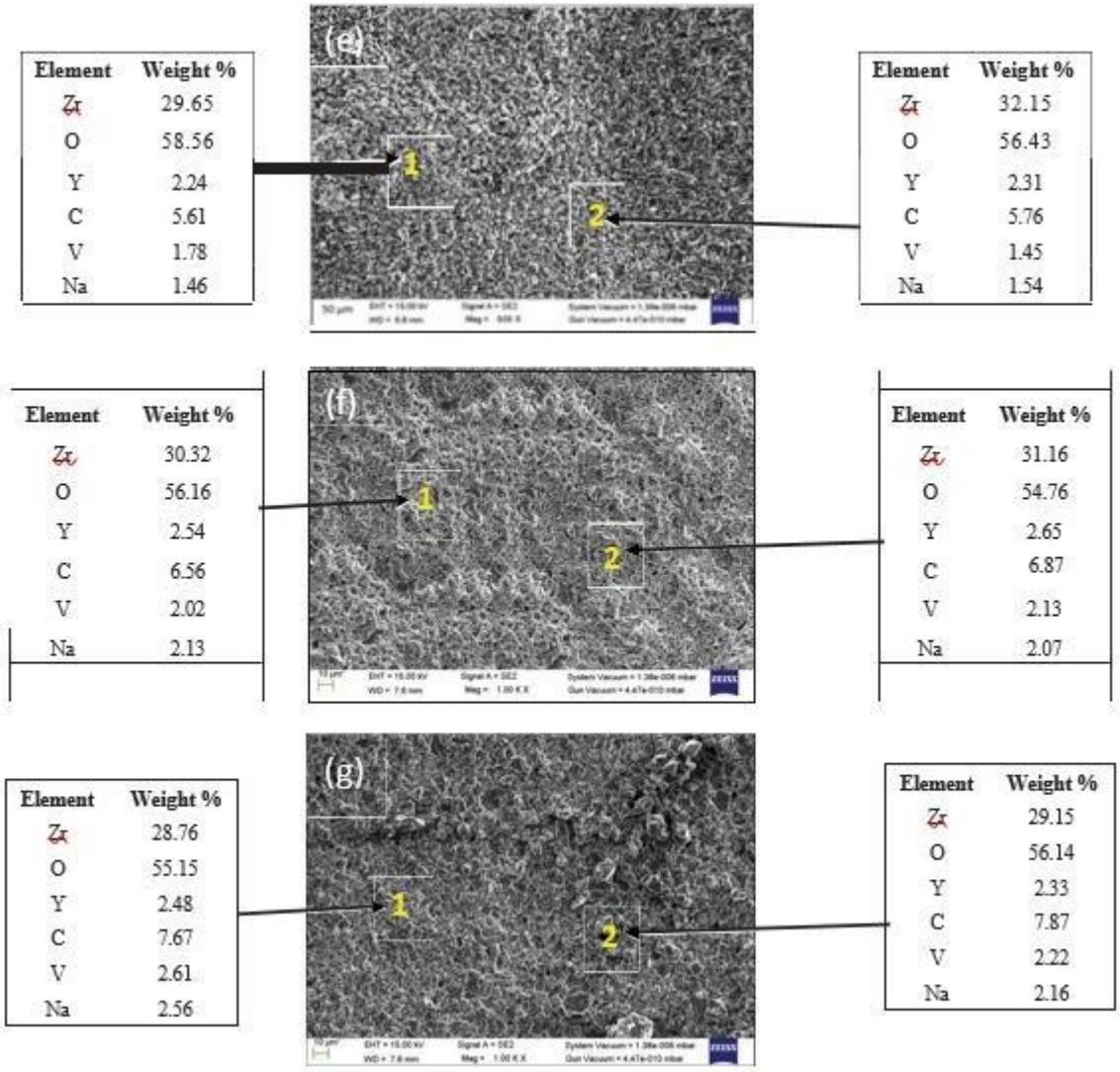

Figure 8. SEM/EDAX analysis of : (a) un-coated; (b) conventional ZrO_2-Y_2O_3; (c) ZrO_2-Y_2O_3–0.5Wt.%CNT; (d) ZrO_2-Y_2O_3-1Wt.%CNT; (e) ZrO_2-Y_2O_3–2Wt.%CNT; (f) ZrO_2-Y_2O_3–4Wt.%CNT; (g) ZrO_2-Y_2O_3–6Wt.%CNT-coated T-91 steel samples after hot corrosion at 900°C.

ZrO_2-Y_2O_3-1 wt.% CNT-Coated T-91 Steel

In the case of the 1 wt.% CNT-reinforced coating (Figure 8(d)), the oxide scale displayed a nodular microstructure with minor irregular flakes. EDAX analysis showed a composition predominantly of Zr and O, along with significant carbon and traces of Na and V. The findings indicated that CNTs remained intact within the coating, enhancing its protective properties.

ZrO_2-Y_2O_3-2 wt.%, 4 wt.%, and 6 wt.% CNT-Coated T-91 Steel

The SEM images for specimens with 2 wt.%, 4 wt.%, and 6 wt.% CNT-reinforced coatings (Figures 8(e), 8(f), and 8(g)) revealed uniform and intact oxide scales with regular morphologies. EDAX analysis consistently showed high percentages of Zr and O, with substantial carbon content confirming the presence of CNTs. The oxide scale remained dense and spallation-free, indicating excellent protection against hot corrosion. The 6 wt.% CNT coating demonstrated the best performance, forming a highly stable and uniform protective layer.

3.5 Cross-Sectional Analysis

The cross-sectional micrographs from SEM and elemental analyses for uncoated, conventional ZrO_2-Y_2O_3-coated, and CNT-reinforced ZrO_2-Y_2O_3-coated T-91 steel specimens after hot corrosion testing at 900°C for 50 cycles are shown in Figure 9. These analyses provide insight into the structural integrity and elemental composition of the oxide scales and coatings.

Uncoated T-91 Steel

The cross-sectional SEM analysis of the uncoated T-91 steel revealed a porous structure, allowing corrosive species to easily infiltrate the substrate. Elemental analysis at specific points confirmed a high concentration of Fe and O in the oxide scale, with minor amounts of Na, V, Cr, and Mo. The oxide layer was primarily composed of Fe_2O_3, which is non-protective in nature and prone to cracking. The poor adherence of this porous oxide scale led to rapid material degradation during cyclic exposure.

Conventional ZrO_2-Y_2O_3-Coated T-91 Steel

For the conventional ZrO_2-Y_2O_3 coating, the cross-sectional analysis showed a somewhat adherent oxide scale with fewer cracks compared to the uncoated specimen. However, cracks and voids were observed in localized regions of the scale, suggesting vulnerability to penetration by molten salts. Elemental analysis detected Zr, Fe, and O as primary constituents, indicating the formation of zirconium oxides alongside iron oxides. The presence of molten salt elements such as Na and V was also confirmed, suggesting infiltration through the cracks in the oxide layer.

CNT-Reinforced ZrO_2-Y_2O_3-Coated T-91 Steel

The cross-sectional SEM micrographs for CNT-reinforced coatings (0.5 wt.%, 1 wt.%, 2 wt.%, 4 wt.%, and 6 wt.% CNT) revealed a dense and uniform structure across the oxide scale, with no visible cracks or spallation. The oxide layers were adherent and smooth, indicating excellent corrosion resistance. Elemental analysis showed significant amounts of Zr and O, with the presence of carbon confirming the retention of CNTs in the coating matrix. As the CNT content increased, porosity decreased, resulting in enhanced resistance to molten salt penetration.

4. Discussion

The plasma spray technique successfully deposited ZrO_2-Y_2O_3 coatings with varying CNT content on T-91 boiler steel. The coating thicknesses ranged from 250–270 µm, with porosity levels decreasing from 4.25% in conventional coatings to significantly lower values in CNT-reinforced coatings.

Uncoated Steel

Uncoated T-91 steel underwent severe oxidation, with porous Fe_2O_3 scales forming after the second cycle of hot corrosion. Cracks in the oxide layer allowed oxygen and molten salts to penetrate the substrate, leading to cumulative weight gains of 399.12 mg/cm² after 50 cycles and a high parabolic rate constant (K_p = 8,849.82 × 10^{-10} g^2 cm^{-4} s^{-1}). These findings align with previous studies on boiler steels under similar conditions (El-Awadi et al., 2016; Rani et al., 2017).

Conventional Coatings

Conventional ZrO_2-Y_2O_3 coatings reduced weight gain by 87.21% compared to uncoated steel, with a cumulative gain of 51.03 mg/cm² and a lower K_p of 144.67 × 10^{-10} g^2 cm^{-4} s^{-1}. Despite this improvement, cracks and spallation were observed due to thermal cycling stresses, as reported by Goyal et al. (2018a) and Chatha et al. (2012). These cracks allowed molten salts to reach the substrate, leading to localized degradation.

CNT-Reinforced Coatings

CNT-reinforced coatings demonstrated significantly improved performance. Weight gains for the coatings decreased progressively with increasing CNT content, with 6 wt.% CNT coatings achieving the lowest gain of 8.81 mg/cm²—representing a 97.79% reduction compared to uncoated steel. The parabolic rate constant ($K_p = 4.31 \times 10^{-10}$ g² cm⁻⁴ s⁻¹) was the lowest among all samples, indicating minimal corrosion rates.

The addition of CNTs enhanced the coatings by:

1. **Filling Voids and Reducing Porosity:** CNTs filled microvoids in the coating matrix, acting as barriers to molten salts and oxygen diffusion.
2. **Improving Thermal Properties:** CNTs increased the heat absorption capacity, uniformly distributing heat and reducing thermal stresses, as noted by Keshri and Agarwal (2011).
3. **Enhancing Mechanical Stability:** The dense and crack-free structure of CNT-reinforced coatings resisted spallation during cyclic thermal stress.

XRD and EDAX analyses confirmed the presence of CNTs in the coatings, even after prolonged exposure. The formation of protective ZrO_2-Y_2O_3 and stable carbon-rich layers provided effective resistance against corrosive species. These findings corroborate studies by Ahmad et al. (2010) and Singhal et al. (2012), which reported similar improvements with

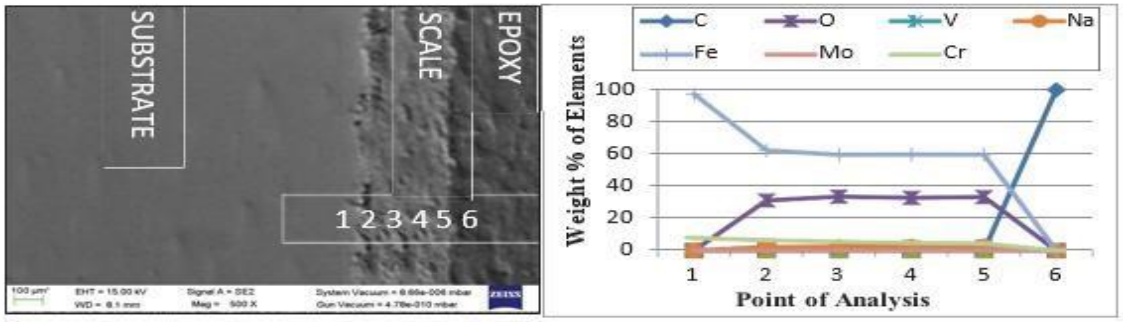
SUBSTRATE
SCALE
EPOXY
1 2 3 4 5 6
C
O
V
Na
Fe
Mo
Cr
Weight % of Elements
Point of Analysis

(a)

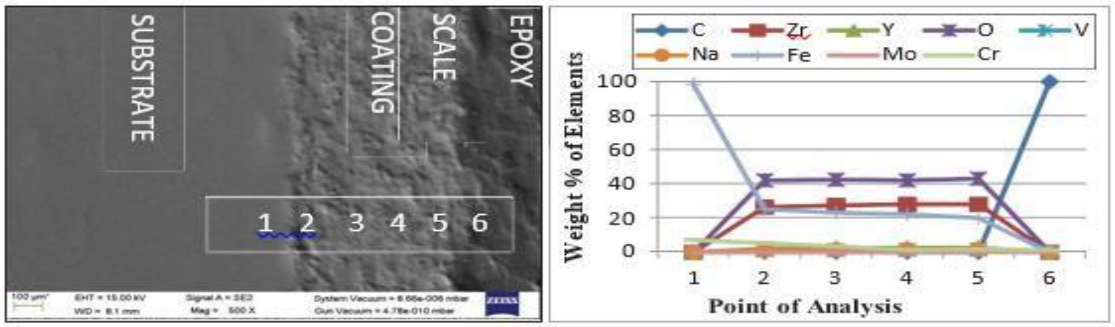
SUBSTRATE
COATING
SCALE
EPOXY
1 2 3 4 5 6
C
Zr
Y
O
V
Na
Fe
Mo
Cr
Weight % of Elements
Point of Analysis

(b)

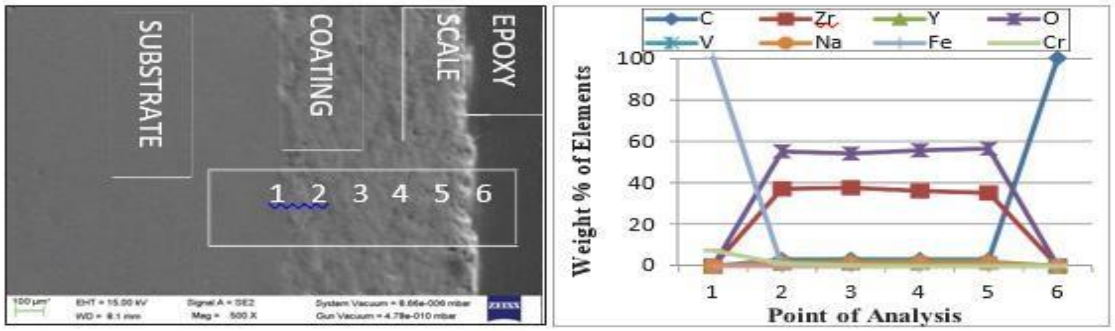
SUBSTRATE
COATING
SCALE
EPOXY
1 2 3 4 5 6
C
Zr
Y
O
V
Na
Fe
Cr
Weight % of Elements
Point of Analysis

(c)

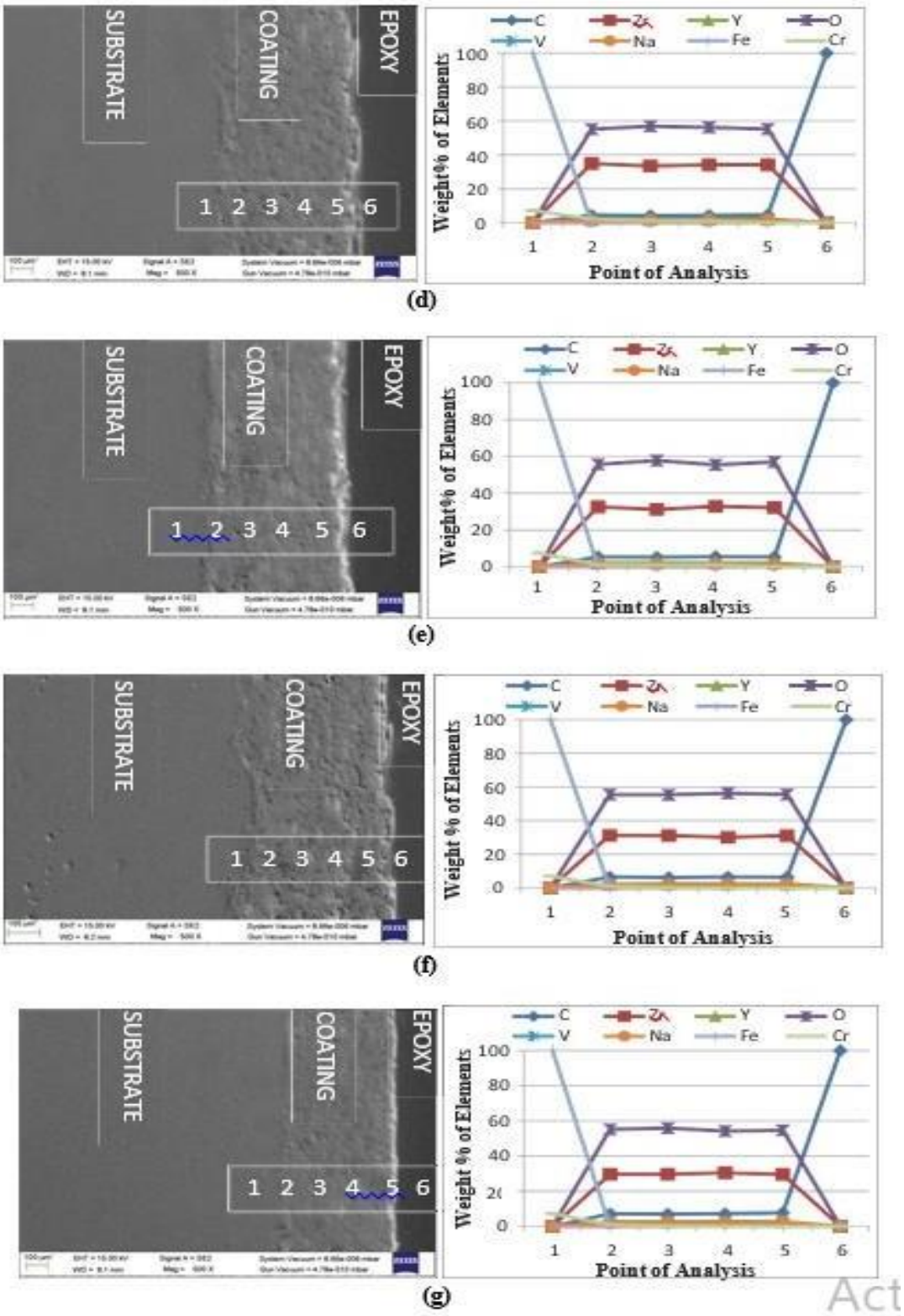

Figure 9 . Cross-sectional morphology along with elemental composition of (a) un-coated; (b) conventional ZrO_2-Y_2O_3; (c) ZrO_2-Y_2O_3–0.5Wt.%CNT; (d) ZrO_2-Y_2O_3–1Wt.%CNT; (e) ZrO_2-Y_2O_3–2Wt.%CNT; (f) ZrO_2-Y_2O_3– 4Wt.%CNT; (g) ZrO_2-Y_2O_3–6Wt.%CNT- coated T-91 steel samples after hot corrosion at 900°C

5. Conclusions

- The study examined the hot corrosion behavior of CNT-reinforced ZrO_2-Y_2O_3 coatings on T-91 steel at 900°C in a molten salt environment (Na_2SO_4 – 60 wt.% V_2O_5). The uncoated T-91 steel showed the highest weight gain and corrosion rate, forming a non-protective, porous, and thick oxide scale that accelerated material degradation.
- Conventional ZrO_2-Y_2O_3 coatings significantly reduced weight gain compared to the uncoated steel. However, cracks and minimal thermal spallation were observed during initial exposure cycles, and the coating eventually delaminated in later cycles due to thermal stress.
- CNT-reinforced ZrO_2-Y_2O_3 coatings exhibited markedly lower weight gain compared to both uncoated and conventional ZrO_2-Y_2O_3-coated T-91 steel specimens. These coatings remained intact, free of cracks, and showed no spallation throughout the testing period.
- XRD analysis confirmed the formation of a protective ZrO_2-Y_2O_3 oxide layer in the CNT-based coatings, with additional peaks indicating carbon retention in the matrix. Increasing CNT content in the coating matrix significantly enhanced the hot corrosion resistance of T-91 steel, demonstrating superior performance over conventional coatings.

This research highlights the potential of CNT-reinforced ZrO_2-Y_2O_3 composite coatings as an effective solution for improving the durability of boiler steel under high-temperature corrosive environments.

References

[1] Ahmad, I., Unwin, M., Cao, H., Chen, H., Zhao, H., Kennedy, A. and Zhu, Y.Q. (2010), "Multi-walled carbon nanotubes reinforced Al2O3 nanocomposites: mechanical properties and interfacial investigations", *Composites Science and Technology*, Vol. 70 No. 8, doi: 10.1016/j. compscitech.2010.03.007.

[2] Alia, F.F., Kurniawan, T., Asmara, Y.P., Ani, M.H.B. and Nandiyanto, A.B.D.(2017a),"High temperature oxidation in boiler environment of chromized steel", *IOP Conference Series:Materials Science and Engineering*,Vol.257 No.1,doi: 10.1088/1757-899X/257/1/012086.

[3] Alia, F.F., Kurniawan, T., Asmara, Y.P., Ani, M.H.B. and Nandiyanto, A.B.D. (2017b), "High temperature oxidation in boiler environment of chromized steel", *IOP Conference Series:Materials Science and Engineering*,Vol.257 No.1, doi: 10.1088/1757-899X/257/1/012086.

[4] Bengtsson,P. and Johannesson,T.(1995), "Characterization of micro structural defects in plasma-sprayed thermal barrier coatings", *Journal of Thermal Spray Technology*, Vol. 4No.3, pp.245-251,doi:10.1007/BF02646967.

[5] Chatha, S.S., Sidhu, H.S. and Sidhu, B.S. (2012), "High temperaturehotcorrosionbehaviourofNiCrandCr3C2- NiCr coatings on T91 boiler steel in an aggressive environmentat750°C",*SurfaceandCoatingsTechnology*, Vol.206Nos19/20,pp.3839-3850,doi:10.1016/j.surfcoat.2012.01.060.

[6] El-Awadi,G.A.,Abdel-Samad,S.andElshazly,E.S.(2016), "Hot corrosion behavior of Ni based inconel 617 and inconel 738superalloys",*Applied Surface*

Science,Vol.378,pp.224-230,doi:10.1016/j.apsusc.2016.03.181.

[7] Eliaz, N., Shemesh, G. and Latanision, R.M. (2002), "Hot corrosion in gas turbine components", *Engineering Failure Analysis*,Vol.9 No.1,pp.31-43.

[8] Erickson, L.C., Westergård, R., Wiklund, U., Axen, N., Hawthorne, H.M. and Hogmark, S. (1998), "Cohesion in plasma-sprayed coatings – a comparison between evaluation methods", *Wear*, Vol. 214 No. 1, pp. 30-37.

[9] Gell,M., Wang,J., Kumar,R., Roth,J., Jiang,C. and Jordan,E.H. (2018), "Higher temperature thermal barrier coatings with the combined use of yttrium aluminum garnet and the solution precursor plasma spray process", *Journal of Thermal Spray Technology*, Vol. 27 No. 4, pp. 543-555, doi: 10.1007/s11666-018-0701-7.

[10] Gond, D., Chawla, V., Puri, D., Prakash, S., Electrical, H., Plant, E., Heavy, B. and Limited, E. (2010), "Oxidation studies of T-91 and T-22 boiler steels in air at 900° C", *Journal of Minerals and Materials Characterization and Engineering*, Vol. 9 No. 8, pp. 749-761.

[11] Goyal, K. (2018a), "Experimental investigations of carbon nanotubes reinforcement on properties of ceramic-based composite coating".

[12] Goyal, K. and Goyal, R. (2020), "Improving hot corrosion resistance of Cr3C2–20NiCr coatings with CNT reinforcements", *Surface Engineering*, Vol.36No.11, pp.1200-1209.

[13]Goyal, R., Sidhu, B.S.and Chawla, V. (2017), "Characterization of plasma-sprayed carbon nanotube (CNT)-reinforced alumina coatings on ASME-SA213-T11 boiler tube steel", *The International Journal of Advanced Manufacturing Technology*, Vol. 92 Nos 9/12, pp. 3225-3235.

[14]Goyal,R., Sidhu,B.S. and Chawla,V. (2018a), "Improving the high-temperature oxidation resistance of ASME-SA213-T11 boiler tube steel by plasma spraying with CNT-reinforced alumina coatings", *Anti-Corrosion Methods and Materials*, Vol.65No.2.

[15] Goyal, R., Sidhu, B.S. and Chawla, V. (2018b), "Oxidation behaviour of plasma sprayed carbon nanotubes-alumina coated ASME-SA213-T291 boiler tube steel", *Journal of Material & Metallurgical Engineering*, Vol.7 No.3, pp.1-15.

[16] Goyal, K., Singh, H. and Bhatia, R. (2018), "Cyclic high temperature corrosion studies of carbon nanotubes-Cr2O3 composite coatings on boiler steel at 900°C in molten salt environment", *Anti-Corrosion Methods and Materials*, Vol. 65 No. 6, pp. 646-657, doi: 10.1108/ACMM-06-2018-1954.

[17] Goyal, K., Singh, H. and Bhatia, R. (2019), "Hot-corrosion behavior of Cr2O3-CNT-coated ASTM-SA213-T22 steel in a molten salt environment at 700°C", *International Journal of Minerals, Metallurgy, and Materials*, Vol.26 No.3, pp.337-344,doi:10.1007/s12613-019-1742-8.

[18] Guo, W. and Tam, H.Y. (2014), "Effects of carbon nanotubes onwear of WC/Co micropunches", *The International Journal of Advanced Manufacturing Technology*, Vol.72 Nos1/4, pp.269-275,doi:10.1007/s00170-014-5661-6.

[19] Gutierrez-Gonzalez, C.F., Smirnov, A., Centeno, A., Fern´andez, A., Alonso, B., Rocha, V.G., Torrecillas, R., Zurutuza, A. and Bartolome,J.F. (2015), "Wear behavior of graphene/alumina composite", *Ceramics International*, Vol. 41 No. 6, doi: 10.1016/j.ceramint.2015.02.061.

[20] Habibi, M.H. and Guo, S.M. (2015), "The hot corrosion behavior of plasma sprayed zirconia coatings stabilized with yttria, ceria, and titania in sodium sulfate and vanadium oxide", *Materials and Corrosion*, Vol. 66 No. 3, pp. 270-277.

[21] Iijima,S. (1991), "1991 nature publishing group.", *Nature*, Vol. 354 No. 6348, pp. 56-58.

[22] Jambagi, S.C. and Bandyopadhyay, P.P. (2017), "Plasma sprayed carbon nanotube reinforced splats and coatings", *Journal of the European Ceramic Society*, Vol.37 No.5, pp.2235-2244.

[23] Jiang, C.P., Xing, Y.Z., Zhang, F.Y. and Hao, J.M. (2012), "Micro structure and corrosion resistance of Fe/Mo composite amorphous coatings prepared by air plasma spraying", *International Journal of Minerals, Metallurgy, and Materials*, Vol.19 No.7, pp.657-662, doi:10.1007/s12613-012-0609-z.

[24] Kamal, S., Jayaganthan, R. and Prakash, S. (2009), "Evaluation of cyclic hot corrosion behavior of detonation gun sprayed Cr3C2-25%Ni Cr coatings on nickel-andiron- based super alloys", *Surface and Coatings Technology*, Vol.203 No.8, pp.1004-1013, doi:10.1016/j.surfcoat.2008.09.031.

[25] Katiki, K., Yadlapati, S., Chidepudi, S.N.S. and Hari, P.R. (2014), "Comparative high temperature corrosion studies on zirconium dioxide coated inconel 625 in air and molten salt environment", *Int J Chem Tech Res*, Vol.6, pp.4579-45845.

[26] Keshri, A.K. and Agarwal, A. (2011), "Splat morphology of plasma sprayed aluminum oxide reinforced with carbon nanotubes: a comparison between experiments and simulation", *Surface and Coatings Technology*, Vol.206 Nos2/3, doi:10.1016/j.surfcoat.2011.07.025.

[27] Kumar, S., Bhatia, R. and Singh, H. (2020a), "Hot corrosion behavior of CNT-reinforced zirconium yttrium composite coating at elevated temperature", *Materials Today: Proceedings*,Vol.28, doi:10.1016/j.matpr.2020.04.836.

[28] Kumar, S.,Bhatia, R. and Singh, H. (2020b),"Hotcorrosion behavior of CNT reinforced zirconium yttrium coatings in molten salt environment", *Journal of Bio- and Tribo- Corrosion*,Vol.6 No.3, doi:10.1007/s40735-020-00378-3.

[29] Loghman-Estarki, M.R., Shoja Razavi, R., Edris, H., Bakhshi, S. R., Nejati, M. and Jamali, H. (2016), "Comparison of hot corrosion behavior of nano structured Sc YSZ and YSZ thermal barrier coatings", *Ceramics International*, Vol.42 No.6, pp.7432-7439, doi:10.1016/j.ceramint.2016.01.147.

[30] Mehta,J.,Mittal,V.K.andGupta,P.(2017),"Roleofthermal spray coatings on wear, erosion and corrosion behavior: a review", *Journal of Applied Science and Engineering*, Vol. 20 No. 4, pp. 445-452, doi: 10.6180/jase.2017.20.4.05.

[31] Rani,A., Bala,N. And Gupta, C.M. (2017), "Characterization and hot corrosion behavior of D-gun sprayed Cr2O3-75% Al2O3 coated ASTM-SA210-A1 boiler steel in molten salt environment", *Anti-Corrosion Methods and Materials*, Vol. 64 No. 5, pp. 515-528, doi: 10.1108/ACMM-09-2016-1712.

[32] Rezakhani, D. (2007), "Corrosion behaviours of several thermal spray coatings used on boiler tubes at elevated temperatures", *Anti-Corrosion Methods*

and Materials, Vol. 54 No. 4, pp. 237-243, doi: 10.1108/00035590710762384.

[33] Saremi, M., Afrasiabi, A. and Kobayashi, A. (2008), "Microstructural analysis of YSZ and YSZ/Al2O3 plasma sprayed thermal barrier coatings after high temperature oxidation", *Surface and Coatings Technology*, Vol.202 No.14, doi:10.1016/j.surfcoat.2007.11.029.

[34] Schroeder,M. And Unger,R. (1997),"Thermal spray coatings replace hard chrome", *Advanced Materials &Processes*, Vol. 152 No. 2, pp. 19-21.

[35] Sidhu, B.S. and Prakash, S. (2005), "High-temperature oxidation behavior of NiCrA1Y bond coats and stellite-6 plasma-sprayed coatings", *Oxidation of Metals*, Vol. 63 Nos 3/4, pp. 241-259.

[36] Sidhu,V.P.S., Goyal,K. and Goyal,R. (2017), "Comparative study of corrosion behaviour of HVOF-coated boiler steel in actual boiler environment of a thermal power plant", *Journal of the Australian Ceramic Society*, Vol. 53 No. 2, pp. 925-932, doi:10.1007/s41779-017-0107-x.

[37] Singh,A., Goyal,K., Goyal,R. and Krishan,B. (2021), "Hot corrosion behavior of different ceramics coatings on boiler tube steel at 800°C temperature", *Journal of Bio-and Tribo- Corrosion*,Vol.7No.1,pp.1-9.

[38] Singh, G., Goyal, K. and Bhatia, R. (2018), "Hot corrosion studies of plasma-sprayed chromium oxide coatings on boiler tube steel at 850 C in simulated boiler environment Iranian", *Journal of Science and Technology, Transactions of Mechanical Engineering*, Vol. 42 No. 2, pp. 149-159.

[39] Singhal,S.K., Pasricha,R., Jangra,M., Chahal,R., Teotia,S. and Mathur, R.B. (2012), "Carbon nanotubes: amino functionalization and its application in the fabrication of Al- matrix composites", *Powder Technology*, Vols 215/216, doi: 10.1016/j.powtec.2011.10.013.